Supplementary materials

1 Chemical composition of pre-alloyed powders

Table S1 Chemical composition analysis for the CoCrFeMnNi matrix and NiCoFeAlTi reinforcement wt.%

Composite	Co	Cr	Fe	Mn	Ni	Al	Ti
CoCrFeMnNi	20.51	19.23	20.36	19.68	20.22	0	0
NiCoFeAlTi	26.16	0	9.28	0	51.41	0.56	12.59

2 Microstructures of CoCrFeMnNi high entropy alloy before and after aging

Figure S1 presents the micrographs of CoCrFeMnNi HEA before and after aging at different temperatures. As shown in Figure S1(a), the as-printed HEA exhibits a microstructure composed of both columnar and equiaxed subgrains, with subgrain sizes of ~0.41 μm and ~0.45 μm, respectively. After aging at 873 K (Figure S1(b)), the presence of columnar and equiaxed subgrains disappears. However, the presence of grain boundaries can be observed, and the voids represent localized corrosion during metallographic etching. When the aging temperature increases to 1073 K (Figure S1(c)), both columnar and equiaxed subgrains disappear entirely. With further increase in the aging temperature (Figures S1(d) and (e)), the alloy exhibits continuous precipitates along the grain boundaries caused by high-temperature oxidation, and the size of these precipitates increases with temperature.

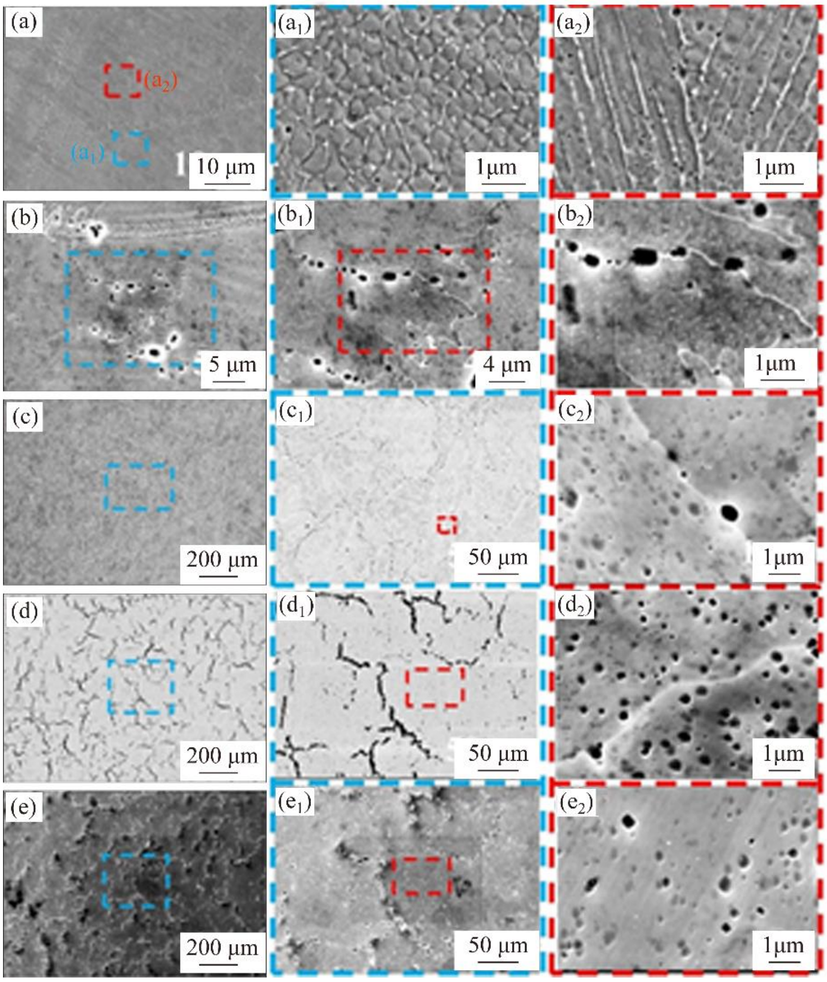

Figure S1 Microstructures of CoCrFeMnNi high entropy alloy before (a, a_1, a_2) and after aging in aged conditions of 873 K (b, b_1, b_2), 1073 K (c, c_1, c_2), 1273 K (d, d_1, d_2), and 1423 K (e, e_1, e_2)

3 EDS spectrum of nanoscale precipitates in HEACs after aging

Figure S2 presents the EDS point analysis of the nanoscale precipitates in the HEACs after heat treatment at 1423 K for 2 h. To ensure data reliability, we randomly selected three positions within the nanoprecipitates (red dashed circles) and the matrix (yellow dashed circles) for point energy spectroscopy analysis. The corresponding chemical compositions are statistically presented in Table S2). The results indicate that the nanoscale precipitates are enriched in Al and Ti, while no Al and Ti are detected in the matrix. This suggests that nearly all the Al and Ti, which were originally dissolved in the matrix, have precipitated after aging at 1423 K for 2 h.

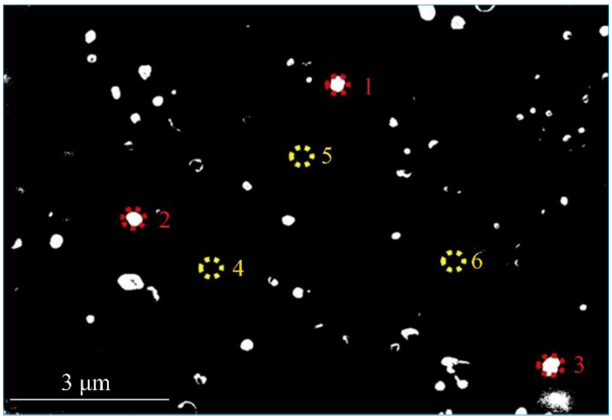

Figure S2 EDS spectrum of nanoscale precipitates in HEAC with HER after aging at 1423 K for 2 h

Table S2 Chemical composition distribution in HEAC with HER in different regions after aging at 1423 K for 2 h

at.%

Point	Al	Ti	Cr	Mn	Fe	Co	Ni
1	4.36	0.83	21.01	18.22	19.61	19.69	19.29
2	6.23	0.18	22.16	22.23	20.16	17.88	16.37
3	3.66	0.14	21.43	18.39	20.6	19.78	19.65
4	0	0	20.57	20.14	20.24	19.72	19.30
5	0	0	19.33	23.30	19.36	19.21	18.80
6	0	0	21.36	19.06	20.33	19.36	18.99

4 Tensile fracture morphologies of CoCrFeMnNi HEA matrix and HEACs before and after aging

Figure S3 displays the tensile fracture surface morphologies for the CoCrFeMnNi HEA before and after aging as a function of varying temperatures. It can be observed that there are inclined microfacets growing upwards on the fracture surface of CoCrFeMnNi HEA (Figure S3(a)). Microcracks exist at the bottom of the fracture surface, which may be caused by the propagation of cracks parallel to the tensile direction. Some micropores can be observed in relatively flat regions (Figure S3(a_1)). Upon magnification, dense notches can be observed, with uneven growth angles and sizes. In some notch-like features, spherical particles are present (Figure S3(a_2)), which may be nanoscale oxides formed during the printing process. As shown in Figure S3(b), after aging at 873 K, the notch-like features reduce, and the surface tends to be coherent. This may be attributed to the release of residual stresses during heat treatment. It can be observed in the magnified image that the number of micropores decreases (Figures S3(b_1) and (b_2)), which may be attributed to the growth of nanoscale oxide particles during the heat treatment. After heat treatment at 1073 K (Figure S3(c)), cracks and micropores almost disappear due to recrystallization. The size of the notch increases, with a fine toughness notch along grain boundaries and a coarse notch along the center (Figure S3(c_3)). This may be caused by the ease of introducing nanoscale oxides along grain boundaries during non-vacuum heat treatment, while oxides formed inside grains during the printing process grow larger. The size of the notch-like feature is determined by the particles within, resulting in small notch-like features along grain boundaries. As shown in Figure S3(d_2), with increasing heat treatment temperature to 1273 K, there is a variation in dimple distribution. Fine dimples are observed along certain regions (Area A) surrounded by larger dimples (Area B). When the heat treatment temperature reaches 1423 K, the dimples exhibit rapid growth and uniform distribution (Figure S3(e_2)). This indicates complete recrystallization of the HEA and uniform distribution of oxides. In summary, as the heat treatment temperature increases, the HEA exhibits higher ductility, and the dimple morphology is influenced by the size and distribution of oxides.

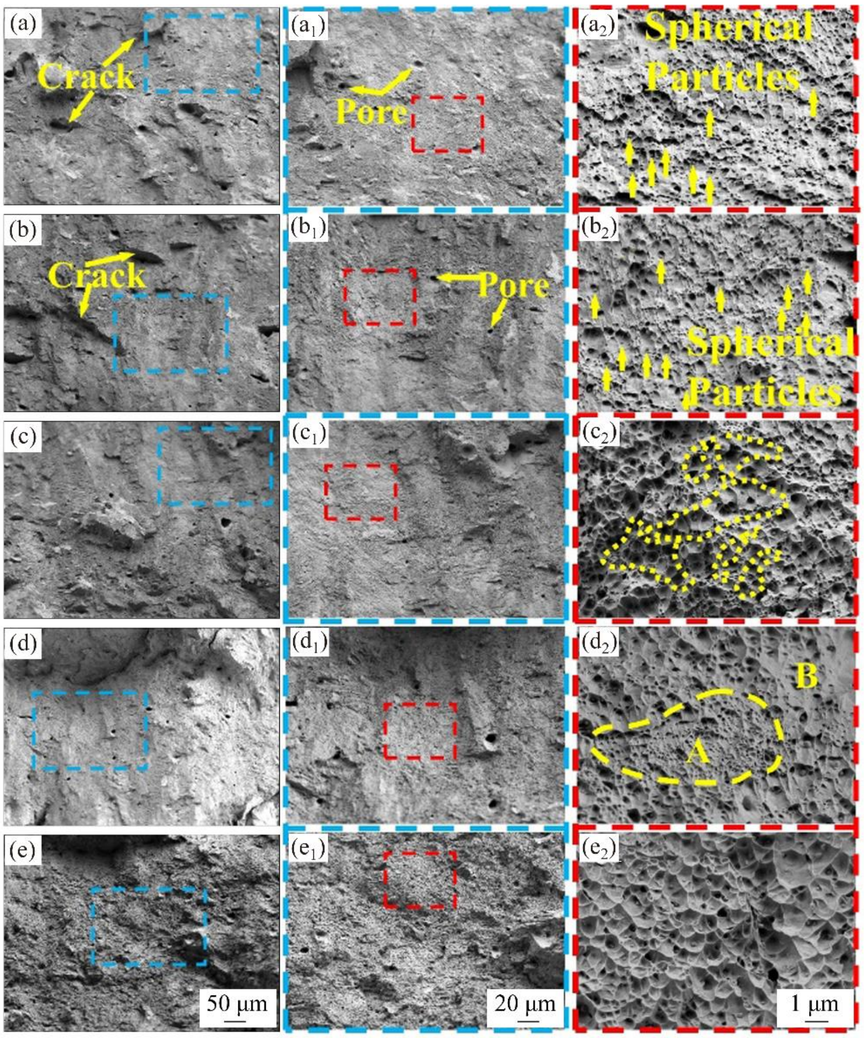

Figure S3 Tensile fracture morphologies of the CoCrFeMnNi HEA matrix before (a, a_1, a_2) and after aging in aged conditions of 873 K (b, b_1, b_2), 1073 K (c, c_1, c_2), 1273 K (d, d_1, d_2), and 1423 K (e, e_1, e_2)

The room temperature tensile fracture surface morphologies of HEACs with HER are shown in Figure S4. From Figure S4(a), it can be observed that there are numerous voids and microcracks in the HEAC, and the voids may have formed due to the coalescence of micropores. The distribution of dimples is relatively uniform, with smaller oxide particles present near larger dimples as shown in Figure S4(a_2). After aging at 873 K, the fracture surface exhibits more interconnected voids and cracks, which may be due to the presence of a high degree of residual stresses in the HEACs as compared to the HEA matrix. During aging, relaxation of residual stresses takes place through crack nucleation and propagation, leading to the formation of interconnected cracks and voids (Figure S4(b)). Up on aging at 1073 K, the size and number of cracks and voids in HEACs with HER decrease, which may be attributed to the finer size and more uniform distribution of precipitated Al and Ti-rich phases (Figure S4(c_2)). As the aging temperature increases to 1273 K, the voids disappear (Figure S4(d)) but numerous micropores appear. The HEACs exhibits similar characteristics to HEA (Figure S4(d_2)). The size of dimples continues to increase, with smaller dimples surrounded by larger ones. Figure S4(e_2) displays the dimple morphology of the HEACs with HER after aging at 1423 K, revealing the presence of larger precipitates within the dimples. This may be due to the growth of Al- and Ti-rich particles, as indicated by previous studies on the microstructure [1, 2].

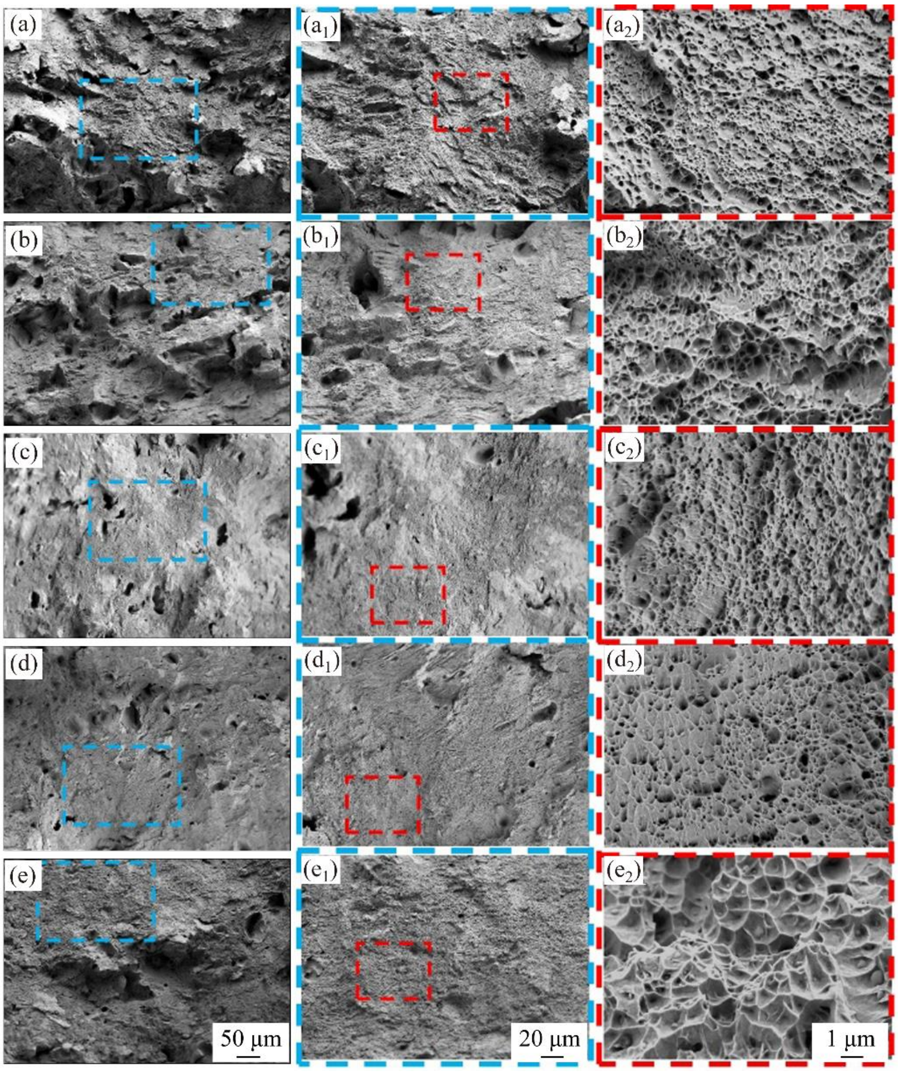

Figure S4 Tensile fracture morphologies of HEACs with HER before (a, a_1, a_2) and after aging in aged conditions of 873 K (b, b_1, b_2), 1073 K (c, c_1, c_2), 1273 K (d, d_1, d_2), and 1423 K (e, e_1, e_2)

5 EBSD analysis of HEACs with HER after aging at 873 K for 2 h

Figure S5 shows the pole figure (PF), inverse pole figure (IPF), and corresponding grain size distribution of the aged HEACs with HER. The results indicate that both HEA and HEACs with HER exhibit a strong texture along the <100> direction after aging (Figures S5(b) and (e)). The maximum texture strength is ~3.37 and ~3.17 for HEA and HEACs with HER, respectively, indicating that HEA has a stronger texture, i.e., a higher preferred orientation tendency, after aging. This is consistent with the previous results, which also showed that both materials have a higher preferred orientation along the <100> direction after aging as revealed by XRD analysis. The IPF plots shown in Figures S5(a) and (d) show the grain distribution, where a more uniform grain distribution is observed for HEA after aging. Therefore, the heterogeneous microstructural features of the HEACs with HER with coarse and fine grains arranged in alternating bands become insignificant. Specifically, the fine grains exhibit preferred growth along the <100> direction, while the coarse grains tend to grow in random directions without any preference. This may be due to the lower energy required for the fine grains to complete recrystallization during the aging [3]. Moreover, previous investigation indicated that the fine grains have a higher density of dislocations resulting from residual stresses, which promote the recrystallization process by consuming dislocation sources [4].

As shown in Figures S5(c) and (f), a statistical analysis of the grain sizes of the two materials after aging indicates that the grain size difference between the HEACs with HER and the HEA is minimal, with average grain sizes of (7.09±0.9) μm and (8.70±0.9) μm, respectively. This indicates that the grain size of HEACs doped with HER did not change significantly. This may be due to the relatively low content of the reinforcing phase. Additionally, the XRD results indicate that the aging led to the solid solution of Al and Ti elements in the HEACs with HER, eliminating macro-segregation, causing lattice distortion, and increasing the lattice constant. The Al and Ti elements in solid solution in the matrix, along with the small-sized Al- and Ti-rich oxide particles, impede grain boundary migration and coalescence, further inhibiting the growth of recrystallized grains.

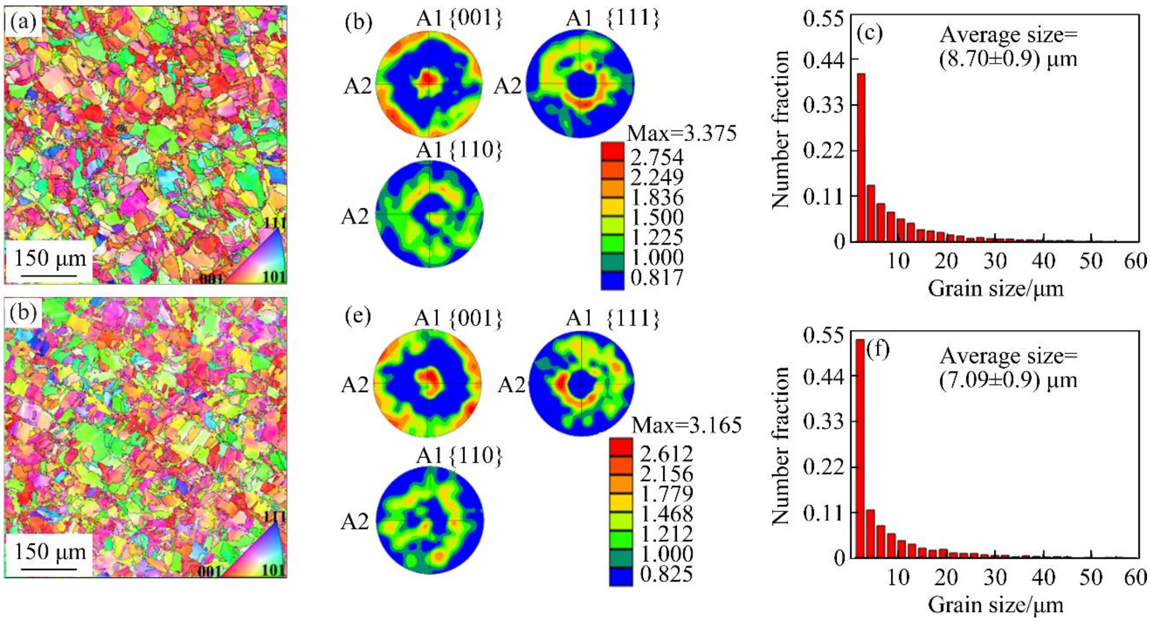

Figure S5 Electron back-scattered diffraction analysis of CoCrFeMnNi HEA (a, b, c) and HEACs (d, e, f) with HER after aging at 873 K for 2 h: (a, d) Inverse polar figure; (b, e) Polar figure; (c, f) Grain size statistics for the HEA and HEACs with HER, respectively

The statistics of high- and low-angle grain boundaries in the aged HEA and HEACs with HER were conducted, as shown in Figure S6. After aging treatment at 873 K, the fraction of low-angle grain boundaries in HEA is approximately 48.4%, as shown in Figure S6(b). The low-angle grain boundaries are distributed within the large-sized grains, while they are nearly absent within the fine grain bands, as shown in Figure S6(a). This indicates that some of the recrystallized grains nucleate and grow by consuming the low-angle grain boundaries within the fine grain bands. In the aged HEACs with HER the fraction of low-angle grain boundaries is higher than in the HEA matrix, at approximately 50.5%, as shown in Figure S6(d). This suggests that the aged HEACs with HER still possess a higher dislocation density. From Figure S6(c), it can be observed that the abundance of low-angle grain boundaries within the fine grain bands disappeared after aging and transformed into high-angle grain boundaries mostly, with low-angle grain boundaries only present inside the large-sized grains. This indicates that the recrystallization process of the HEACs with HER during aging is accomplished by consuming the low-angle grain boundaries within the fine grain bands and transforming them into high-angle grain boundaries.

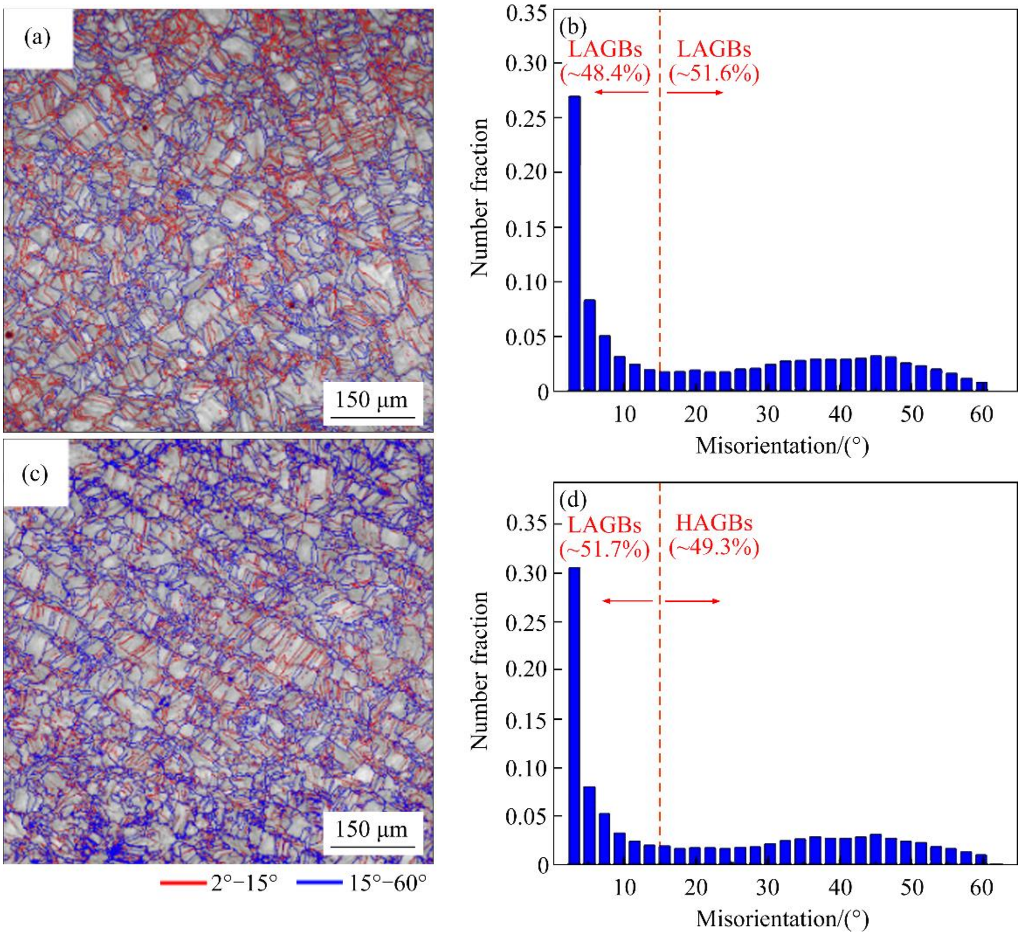

Figure S6 (a, c) Microstructures showing the grain boundary distribution in CoCrFeMnNi HEA and HEACs with HER after aging at 873 K for 2 h and (b, d) their corresponding statistical analysis plots

Figure S7 presents the Kernel average misorientation (KAM) images of the CoCrFeMnNi HEA and HEACs with HER after aging at 873 K for 2 h. The results reveal the presence of high-density dislocations along both low- and high-angle grain boundaries in the aged HEA matrix (Figure S7(a)). In contrast, the aged HEACs with HER exhibit a higher density of dislocations along high-angle grain boundaries (Figure S7(b)). This is likely due to the recrystallization process during aging, which involves the consumption of numerous low-angle grain boundaries and nearby dislocations [5]. Furthermore, the low-angle grain boundaries within large-sized grains undergo a transformation into high-angle grain boundaries, accompanied by the hindered growth of some recrystallized grains due to the presence of second-phase particles [6]. This leads to the accumulation of a substantial amounts of dislocations around these transformed grain boundaries, as revealed by subsequent TEM analysis. From Figure S7(c), it can be concluded that after aging, the average Kernel average misorientation (KAM) value is approximately 0.80 for HEACs with HER and approximately 0.72 for the HEA matrix. This indicates that there is no significant difference in dislocation density between the HEACs with HER and the HEA matrix after aging.

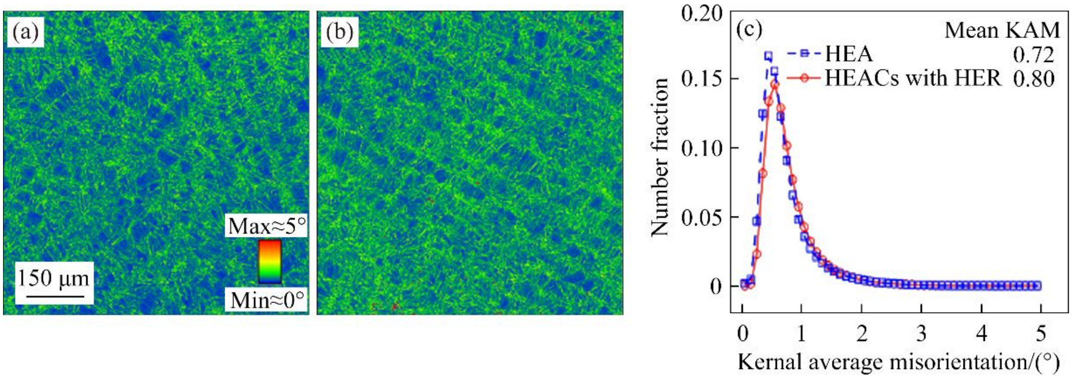

Figure S7 Kernal average misorientation (KAM) map of the (a) CoCrFeMnNi HEA and (b) HEACs with HER after 873 K aging, and (c) the corresponding statistical data

References

[1] ZHAO Y Y, CHEN H W, LU Z P, et al. Thermal stability and coarsening of coherent particles in a precipitation-hardened $(NiCoFeCr)_{94}Ti_2Al_4$ high-entropy alloy [J]. Acta Materialia, 2018, 147: 184−194. DOI: 10.1016/j.actamat.2018.01.049.

[2] QI Yong-liang, CAO Ting-hui, ZONG Hong-xiang, et al. Enhancement of strength-ductility balance of heavy Ti and Al alloyed FeCoNiCr high-entropy alloys *via* boron doping [J]. Journal of Materials Science & Technology, 2021, 75: 154−163. DOI: 10.1016/j.jmst.2020.10.023.

[3] MAN Jia-le, WU Bao-lin, DUAN Guo-sheng, et al. Super-high strength of a CoCrNiFe based high entropy alloy [J]. Journal of Materials Science & Technology, 2024, 177: 79−84. DOI: 10.1016/j.jmst.2023.08.032.

[4] TONG Zhao-peng, ZHANG Yu-ze, LIU Huai-le, et al. Laser shock peening of AlCoCrCuFeNi high-entropy alloy fabricated by laser powder bed fusion: An enhanced oxidation-resistance mechanism at high-temperature [J]. Corrosion Science, 2024, 226: 111667. DOI: 10.1016/j.corsci.2023.111667.

[5] LIU Qian, FANG Lei-ming, XIONG Zheng-wei, et al. The response of dislocations, low angle grain boundaries and high angle grain boundaries at high strain rates [J]. Materials Science and Engineering A, 2021, 822: 141704. DOI: 10.1016/j.msea.2021.141704.

[6] PEI Di, WANG Li, GE Zhi-bao, et al. Microstructure evolution and mechanical properties of Mg-3Al-3Sn-1Zn alloy during multi-pass high-speed rolling [J]. Journal of Alloys and Compounds, 2023, 958: 170406. DOI: 10.1016/j.jallcom.2023.170406.